Desalination and Water Treatment
www.deswater.com

doi: 10.5004/dwt.2018.22781

123 (2018) 288–299
August

Hydrothermally produced activated carbons from zero-cost green sources for cobalt ions removal

George Z. Kyzas[a,*], Eleni A. Deliyanni[b,*], Athanasios C. Mitropoulos[a], Kostas A. Matis[b]

[a]*Hephaestus Advanced Laboratory, Eastern Macedonia and Thrace Institute of Technology, Kavala GR-654 04, Greece, Tel. +30-2510-462247; emails: kyzas@teiemt.gr (G.Z. Kyzas); Tel. +30-2310-997808, lenadj@chem.auth.gr (E.A. Deliyanni)*
[b]*Division of Chemical Technology, Department of Chemistry, Aristotle University of Thessaloniki, Thessaloniki GR-541 24, Greece*

Received 16 March 2018; Accepted 4 July 2018

ABSTRACT

This paper investigates the synthesis of activated carbons with hydrothermal treatment (at three different time intervals 2, 4, and 24 h) from zero-cost sources (potato peels), and activation with H_3PO_4 (at three different temperatures 400°C, 600°C, and 800°C). Characterization techniques used for the study of surface chemistry of carbons prepared (Boehm and potentiometric titrations, Brunauer–Emmett–Teller analysis, scanning electron microscopy/energy dispersive X-ray analysis, and derivative thermogravimetric analysis). The adsorption ability of the prepared activated carbons was evaluated using as model pollutant cobalt ions. Equilibrium and kinetic experiments were carried out at the optimum found pH (6). The carbon sample of 400°C as activation temperature has approximately two times higher adsorption capacity (479 mg/g) than that of 600°C (217 mg/g), while the surface area of the former (466 m^2/g) three times higher than that of 600°C (167 m^2/g). The possible adsorption mechanism was proposed based on Fourier-transform infrared spectra taken after the adsorption of Co(II).

Keywords: Activated carbon; Hydrothermal treatment; Cobalt; Adsorption; Potato peels; Biochars

1. Introduction

Recently, many researchers worldwide turned their interest to the preparation of low-cost adsorbent materials for decontamination/desalination purposes. It is fact that these years there is a question about which adsorbent is most efficient. Some scientists propose adsorbent materials of high adsorption capacity (i.e., >200 mg/g) but with demanding synthesis steps and high-cost. Some other researchers suggest adsorbent materials of medium adsorption capacity (50–200 mg/g) but with simple synthesis routes and really low-cost. Despite the above, many adsorption technology teams worldwide propose for use of the activated carbons prepared by agricultural wastes [1,2].

Activated carbons are widely used in adsorption technology due to their large surface area and different surface functional groups as carboxylic, carbonylic, phenolic, quinonic, lactonic, and/or other groups which are bound to the graphite-like layers [3–5]. For this reason, activated carbons were extensively used as optimum adsorbent materials. Numerous types of activated carbons were produced in the last years for industrial use focusing on the improvement of adsorption capacity given that the cost is kept low [6].

In the present, based on our previous experience/knowledge in activated carbons and low-cost adsorbent materials [1,7–16], hydrothermally prepared activated carbons were produced using potato peels (agro-food wastes) as zero-cost source. The respective hydrothermally treated biochars (hydrochars) were initially synthesized at three different time intervals of hydrothermal treatment (2, 4, and 24 h). These samples (PPH2, PPH4, and PPH24) were fully characterized (SEM, DTG, potentiometric titrations, FTIR, and Brunauer–Emmett–Teller (BET) analysis) and then were further treated by activation with H_3PO_4 at three different temperatures (400°C, 600°C, and 800°C). The latter samples (HP400, HP600, and HP800) were fully characterized

* Corresponding author.

(SEM, DTG, potentiometric titrations, FTIR, and BET analysis) and then their adsorption evaluation was done with experiments of cobalt ions (Co(II)) as model pollutants. Cobalt is a strategic metal (usually obtained from different ores), used widely in the manufacture of catalysts, alloys, steels, etc. Various separation processes were applied for cobalt ions, including radioactive ones [17]. Especially, adsorption as one of the most promising techniques [18–32] is applied for Co(II) removal [33–35]. The use of activated carbon adsorption has been certainly tested in commercial form [36] which was synthesized from a sugarcane industry waste [37] or apricot stone [38]. The novelty of our work is not only the activated carbon samples produced (hydrothermal treatment) but also their application for cobalt ions removal.

2. Materials and methods

2.1. Materials

For the preparation of activated carbons, H_3PO_4 and $Co(NO_3)_2{\cdot}H_2O$ were obtained from Sigma-Aldrich (St. Louis, MO, USA). The potato peels used were obtained as residues/wastes after domestic (home) use.

2.2. Preparation of hydrochars

Potato peels after being washed with distilled water to remove dust and other inorganic impurities were dried overnight at 100°C to reduce the moisture content. The dry material was grounded and sieved to be of uniform particle size (0.45–0.15 mm). The final material was designated as "PP." Hydrochars were firstly treated hydrothermally as follows.

A weighted amount of the dry potato peels precursor (20 g) was dispersed in 100 mL of water. The hydrocarbonization process of the precursor material was carried out in a 1-L Parr stirred pressure reactor (Parr Instrument Company, Moline, Illinois, USA). The mixture was sealed into a Teflon vessel inserted in the autoclave, which was subjected to 200°C at a heating rate of 4°C min/L (pressure at 200°C of around 580 psi) with an agitation speed of 150 rpm. It was maintained at this temperature for different time intervals (2, 4, and 24 h) and after this period of time the autoclave was cooled down to room temperature. The reaction mixture was consisting of a liquid solution and a solid phase (hydrochar); the hydrochar was collected in a glass beaker for separation, was washed thoroughly with hot distilled water followed by ethanol washing, and was dried at 100°C overnight. The solid yield was determined by weight. The hydrochar sample obtained from the feedstock of PP was denoted as "PPH," where "PP" represents the precursor (potato peels) and "H" for the hydrothermal treatment.

2.3. Chemical activation of hydrochars

Chemical activation of the hydrochar was performed using H_3PO_4. The impregnation ratio was calculated as the ratio of the weight of H_3PO_4 in solution to the weight of the used hydrochars (the weight ratio of H_3PO_4/precursor is 1:0.9). The appropriate volume of H_3PO_4 was dissolved in 250 mL of distilled water and then 20 g of the hydrochar was mixed with the H_3PO_4 solution and stirred overnight in order a complete reaction between hydrochar and H_3PO_4 to be achieved. The mixture was filtered and the remaining solid was dried at 100°C for about 24 h. It was placed then in a furnace and heated to 400, 600, and/or 800°C for 2 h at a heating rate of 25°C/min under nitrogen flow (500 mL/min). The activated carbons formed were designated as HP400, HP600, or HP800, respectively. The prepared carbons were Soxhlet washed, freeze-dried, grounded, and sieved. The yield of activated carbons was defined as the ratio of the sample weight after carbonization to the weight of the initial hydrochar.

The whole preparation procedure must be techno-economically evaluated in order to check the real feasibility. However, it is very difficult to approximately estimate the costs, energy, etc. Because in lab-scale experiments, the transportation of raw potato peels was zero. However, in industrial mode, transportation is needed and many other costs. For example, the basic cost in preparation is the energy for the oven (pyrolytic). But either "burn" 1 g of potato peels or 10 g, the energy spent is approximately the same. So, again it cannot be done any clear estimation.

2.4. Characterization techniques

The chemical compositions of the biomass and the hydrochars were determined using elemental analysis. C and H (O content by difference) content of the samples was measured on dry ash free basis and was performed in a vario MACRO cube (Elementar Analysen System GmbH, Germany). The tests for determining the main characteristics of the raw material, the hydrochars and the activated carbons were performed on dry basis according to International Organization for Standardization (ISO) procedures.

The texture characteristics of the resulting activated carbons were determined by nitrogen adsorption/desorption isotherms at 77 K using an automatic adsorption instrument (Quantachrome, Autosorb-1C). Prior to gas adsorption measurements, 0.25 g of each sample was overnight degassed at 200°C in vacuum. The surface area, pore volume, and pore size distribution were determined by the BET and DFT analysis software, respectively. The isotherms were used to calculate the specific surface area, S_{BET}; the total pore volumes (V_t cm^3/g) were estimated to be the liquid volumes of N_2 at a high relative pressure near unity (~0.99), while micropore volume was estimated from *t*-plot. Pore size distribution was obtained by applying the density functional theory (DFT) method [39]. The nonlocal density functional theory (NLDFT) [40,41] provides a method competent to evaluate pore size distributions and predict the pore sizes of activated carbons from simple adsorption data, more reasoned compared with the conventional methods based on the Kelvin equation [42], such as BET [43] and BJH [44] models, taking into consideration the inherent metastability of confined fluid, pore blocking and networking effects, as well as instability of adsorption films and cavitation in condensed fluid, and offering different methods for treating adsorption and desorption isotherms. The main advantages of the DFT method, recommended as the standard method by the International Standard Organization (ISO), are related to its theoretical basis that covers the whole region of micro- and mesopores, applying to different adsorbates

(nitrogen, argon, and carbon dioxide), materials (silicas and carbons), and pore morphologies (slit-like, cylindrical, and spherical).

Surface morphologies were studied by scanning electron microscopy (SEM), performed using JEOL-JSM-6060LV SEM. The surface functional groups were determined by Fourier-transform infrared spectra (FTIR) with a Nicolet 560 (Thermo Fisher Scientific Inc., Boston, MA, USA) FTIR spectrometer. The spectra were recorded in transmission mode using potassium bromate pellets. Thermogravimetric analysis (TGA) was carried out with a Pyris 1 TGA thermal analyzer (Perkin-Elmer, Dresden, Germany) in N_2 atmosphere, at heating rate 10°C/min, and nitrogen flow rate 100 mL/min. Potentiometric titration measurements were carried out with a T50 automatic titrator (Mettler Toledo, Columbia, USA), using $NaNO_3$ solution as supporting electrolyte and NaOH as titration agent, under N_2 atmosphere. The surface charge, Q_{surf} (mmol/g), was calculated by the following equation [45]:

$$Q_{\text{surf}} = \frac{C_A + C_B + [\text{H}^+] + [\text{OH}^-]}{W} \quad (1)$$

where C_A and C_B (mol/L) are the acid and base concentrations, respectively, $[H^+]$ and $[OH^-]$ are the equilibrium concentrations of those ions (mol/L), and W (g/L) is the solid concentration.

2.5. Adsorption experiments

All adsorption experiments were carried out in three repetitions and the average of the values was presented as experimental point in charts. At first, the effect of the pH was determined in batch mode using fixed conditions. 0.02 g of materials (m) were added to 20 mL of adsorbate solution (V) consisted of 100 mg/L initial ion concentrations (C_0). The pH of the solution was fixed to 2, 3, 4, 5, and 6 for each flask by microadditions of HNO_3 (0.01 mol/L) or NaOH (0.01 mol/L). The agitation rate (N) was 150 rpm using thermostatted shaking water bath (model Julabo SW–21C, Seelbach, Germany) under controlled temperature (T = 25°C). The agitation was lasted 24 h (t). pH-effect experiments were not carried out at pH > 6, in order to avoid precipitation phenomena of Co(II). In this pH-region, the residual concentrations of metal ions are due to the formation of colloidal precipitate of metal hydroxide ($Co(OH)_2$) and not due to the adsorption of free metal ions (Co(II)) [46]. After finding the optimum pH of the adsorption (pH 6), the effect of contact time was studied (kinetics). The adsorption experimental conditions were the same (C_0 = 100 mg/L, m = 0.02 g, V = 20 mL, T = 25°C, N = 150 rpm, and pH = 6), but the duration of the adsorption process was studied in fixed-time intervals (t = 5, 10, 15, 20, 30, 45, 60, 90, 120, 150, 180, 240, 300, 360, and 1,440 min). Then, after finding the optimum pH (6) and the optimum contact time (t = 300 min), the effect of the initial ion concentration was also investigated (m = 0.02 g, V = 20 mL, T = 25°C, N = 150 rpm, pH = 6, and t = 300 min). The initial ion concentration was ranged from 10 to 1,000 mg/L. After adsorption, the Co(II) ions were quantitatively analyzed by atomic absorption spectrometer (model Perkin-Elmer Analyst 400, Dresden, Germany) composed of FIAS 100 Flow Injection System. The removal percentage of ions after adsorption was calculated as:

$$R(\%) = \left(\frac{C_0 - C_e}{C_0}\right) \times 100\% \quad (2)$$

where C_0 and C_e (mg/L) are the initial and equilibrium concentration of Co(II) in the aqueous solution.

The equilibrium amount in the solid phase (Q_e, mg/g) was calculated according to the following equation:

$$Q_e = (C_0 - C_e) \times \left(\frac{V}{m}\right) \quad (3)$$

The experimental equilibrium data were fitted to the Langmuir [Eq. (4)] [47], Freundlich [Eq. (5)] [48], and Dubinin–Radushkevich isotherm (Eq. (6)) [49] equations expressed by the following equations:

$$Q_e = Q_m \times \frac{K_L C_e}{1 + K_L C_e} \quad (4)$$

$$Q_e = K_F C_e^{1/n} \quad (5)$$

$$Q_e = Q_m \exp\left[-B_D\left(RT\ln\left(1 + \frac{1}{C_e}\right)\right)^2\right] \quad (6)$$

where Q_m (mg/g) is the maximum amount of adsorption; K_L (L/mg) is the Langmuir adsorption equilibrium constant; K_F ($mg^{1-1/n}$ $L^{1/n}$ g^{-1}) is the Freundlich constant representing the adsorption capacity; n (dimensionless) is the constant depicting the adsorption intensity; B_D (mol^2/kJ^2) is a constant related to the adsorption energy, R (8.314 J/mol/K) is the gas constant, and T (K) is the absolute temperature.

The experimental kinetic data were fitted to two kinetic models; pseudo-first [50] [Eq. (7)], -second order [51] [Eq. (8)], Weber–Morris (Eq. (9)), and Elovich [Eq. (10)] equations (their selection is based on the fact that they are the two most widely-used kinetic models in adsorption works [51,52]).

$$C_t = C_0 - (C_0 - C_e)\left(1 - e^{-k_1 t}\right) \quad (7)$$

$$C_t = C_0 - (C_0 - C_e)\left(1 - \frac{1}{1 + k_2 t}\right) \quad (8)$$

$$Q_t = \frac{1}{b}\ln(a \times b) + \frac{1}{b}\ln(t) \quad (9)$$

$$Q_t = k_{\text{ID}} t^{1/2} + I \quad (10)$$

where k_1 and k_2 (min^{-1}) are the rate constants for the pseudo-first, -second-order kinetic equations; C_0, C_t, and C_e (mg/L) are the initial, transient, and equilibrium concentrations of Co(II) in the aqueous solution, respectively; a (mg/g min) is the initial adsorption rate; b (g/mg) is the desorption

constant; k_{ID} is the intraparticle rate constant; and I is the intercept of the linear fitting.

3. Results and discussion

This section was divided into three major parts: (1) the characterization of hydrochar samples – before activation, (2) the characterization of activated carbons, and (3) the adsorption evaluation of them regarding their adsorption ability to remove Co^{2+} from aqueous solutions.

3.1. Characterizations

3.1.1. Hydrochars

The yield of the hydrochar prepared by the hydrothermal treatment was about 32.5%. The weight loss is mainly attributed to the solubilization of hydrothermal products in the hydrolysis liquors. The carbon content in the hydrochars after the different hydrothermal treatment time, presented in Table 1, increased from 62.4% to 70.0% with the increase of the treatment time. This fraction of the carbon was due to the lignocellulosic biomass that was stored in the hydrochars while the rest carbon content was due to the organic compounds that were dispersed in the hydrolysis liquors (furfural, organic acids, aldehydes, etc.).

The differences of the elemental composition of the prepared hydrothermally-treated hydrochars are illustrated in Fig. 1 (van Krevelen diagram). From this diagram, where the straight lines illustrate the dehydration decarboxylation and demethanation, can be found the process during hydrothermal treatment of the potato peels. The position of the H/C–O/C atomic ratios of the hydrochars suggests that the hydrothermal treatment of the potato peels is a dehydration process as with other lignite-based biomasses.

The hydrothermally obtained hydrochars had a brown color consistent with a partially carbonized product. Inspection of this material by means of microscopy techniques revealed interesting changes in relation to the raw biomass.

SEM images of PP (Fig. 2(a)) show a cellular structure typical of lignocellulosic materials. In contrast, SEM inspection of the hydrochars reveals substantial changes in their surface. Fig. 2 shows representative micrographs corresponding to PP derived hydrochar before activation. From these figures, it can be observed that the hydrochars after 2 h (PPH2) and 4 h (PPH4) hydrothermal treatment keeps the cellular structure of the precursor. Numerous sphere-like microparticles can be seen on the surface of the hydrochar after 24 h hydrothermal treatment (PPH24). These microspheres probably have their origin to the decomposition

Table 1
Carbon and hydrogen content of the hydrochars

Sample	C (%)	H (%)	O (%)
PP	40.1	5.63	37.7
PPH2	62.4	1.62	23.1
PPH4	64.8	2.37	19.4
PPH24	70.0	3.76	15.4

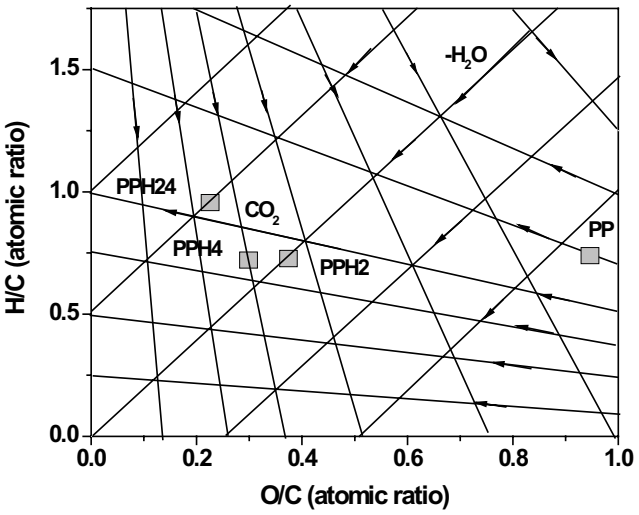

Fig. 1. Van Krevelen diagram; atomic H/C versus O/C ratios for the hydrochars prepared from potato peels.

of cellulose during hydrothermal carbonization, as was recently reported [45], but the reason of their formation as well as the factors influencing their size and composition are not clear. It has been attributed to the gathering of cellulose decomposition compounds [53], or to the loss of water of the microscopic spheres that leads to their further coalescence forming larger spheres [54]. There are fundamental differences in the formation mechanism between the pure carbohydrates particles and the cellulose biomass. In the former case, particles form via a nucleation step from a homogeneous solution through formation and polymerization of hydroxymethylfurfural, while for cellulose/biomass, the fibrous network starts to be disrupted at several points, and nano/microsized cellulose fragments are formed, that since they are not soluble in water, adopt a spherical shape in order to minimize their contacting interface with the surroundings [54]. For lignin, due to its chemical stability, partial degradation occurs, and the original skeleton of the particles is preserved. The morphology of PPH24 seems to indicate that the formation of the microspheres is mainly produced by the breaking-up of cellulose molecules that might be decomposed after an extended time of hydrothermal treatment. Since the cellular structure of the precursor (PP) was presented for PPH2 and PPH4 hydrochars, PPH24 hydrochar was chosen for chemical activation and examination of the activated carbons prepared after activation at different temperatures, as adsorbent material.

Fig. 3 presents DTG (derivative thermogravimetric analysis) curves of the hydrothermally prepared biochars. It should be noted that the samples before thermal analysis were dried at 100°C, so most of the moisture was removed. The hydrochar degradation began with the degradation of hemicellulose (200°C–260°C) followed by the degradation of cellulose (240°C–350°C) and lignine (280°C–500°C) [55,56]. It can be also seen from the DTG curves that in the case of PPH2 and PPH4, there is a process at ~350°C corresponding to the degradation of the fraction of starch and cellulose; for the PPH24 hydrochar this peak was not presented indicating the starch and cellulose degradation after 24 h hydrothermal

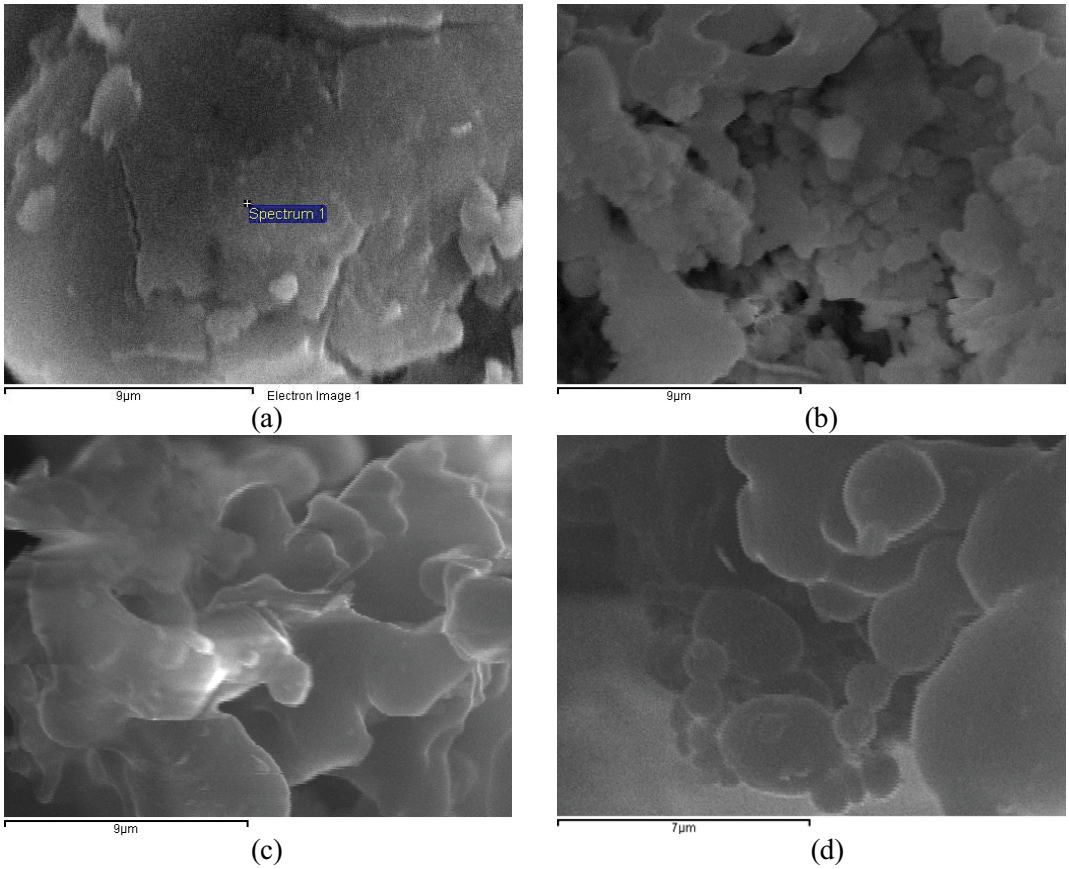

Fig. 2. SEM images of PP (a) and the hydrochars prepared from potato peels after different time of hydrothermal treatment (b) PPH2 (after 2 h); (c) PPH4 (after 4 h); and (d) PPH24 (after 24 h).

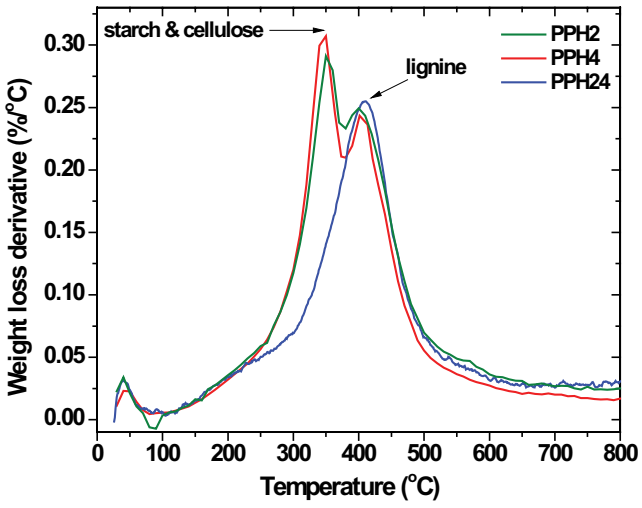

Fig. 3. DTG curves of the hydrothermally prepared biochars.

treatment. In the range of 420°C, the weight loss from lignine degradation was observed for all hydrochars [55,56]. These results are consistent with SEM findings.

The transformations that took place during hydrothermal carbonization of the potato peels were examined with the aid of spectroscopic techniques. The FTIR spectra obtained for the raw material (potato peels) and the corresponding hydrochar samples after different time hydrothermal treatment are presented in Fig. 4.

A detailed analysis of the FTIR spectra of potato peels can be found in the literature [57,58]. The bands identified in the FTIR spectrum of potato peels (for wavenumbers smaller than 2,000 cm^{-1}) were assigned as follows [59]: there are presented absorbencies in the spectra that can be attributed to starch, that is, at 1,160, 1,082, and 1,014 cm^{-1} due to C–O bond stretching [60], to cellulose and hemicellulose, that is, 900 and 1,378 cm^{-1} due to C–H deformation and to lignine, that is, 1,600 and 1,510 cm^{-1} to aromatic ring vibrations of the lignin (the latter mainly in guaiacyl units). Additional characteristic absorption bands at 1,730 and 1,660 cm^{-1} to C=O stretching vibrations (conjugated and nonconjugated keto-carbonyl groups, respectively, due to possible presence of carboxylic acid, ketones, or aldehydes compounds), at 1,435 and 1,240 cm^{-1} due to CH_3 antisymmetry deformation vibration in the carbohydrates and carbonyl C–O stretch vibration, respectively. The FTIR spectra of the hydrochar samples are also shown in Fig. 4. It can be seen that the FTIR spectra of the sample hydrothermally treated at 200°C for 2 h (PPH2) is similar to that of the raw sample, confirming that no chemical transformation occurred. In contrast, the samples corresponding to the hydrochar samples obtained at 200°C for

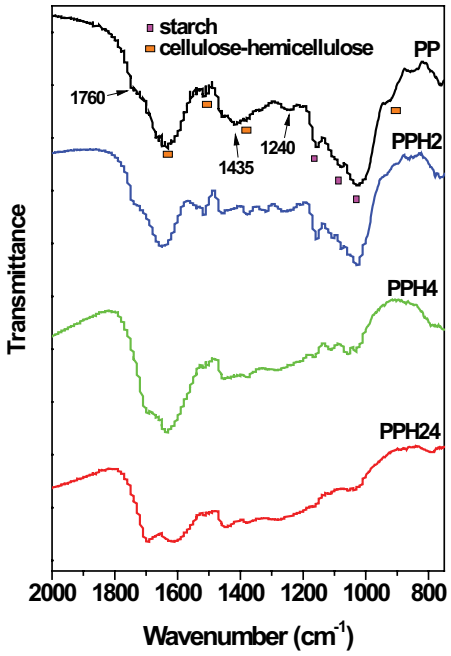

Fig. 4. FTIR spectra of the raw biomass (potato peels) and the hydrochars prepared after different time of hydrothermal treatment.

4 (PPH4) and 24 h (PPH24) exhibited completely different FTIR spectra.

The FTIR spectrum of PPH24 is noteworthy for the absence of bands characteristic of cellulose and hemicellulose such as the bands at 900 and 1,378 cm^{-1} and starch at 1,014 and 1,160 cm^{-1}. In contrast, the bands characteristic of lignin (aromatic structure) are preserved, although they have shifted to lower or higher wavenumbers. Thus, the bands associated to aromatic ring vibrations have shifted to higher wavenumbers, 1,515 and 1,620 cm^{-1}, while the band attributed to C=O vibrations (carbonyl, quinone, ester, or carboxyl) has shifted to a lower wavenumber, that is, 1,710 cm^{-1}. They contain several bands which reveal that aromatization processes take place during hydrothermal carbonization. The presence of aromatic rings is evidenced by the band at 1,620 cm^{-1}, attributed to C=C vibrations [61–63]. The decrease in the intensity of the bands at 1,000–1,460 cm^{-1}, in relation to raw biomass, suggests that dehydration occurred during the hydrothermal carbonization, confirming our analysis of the evolution of the O/C–H/C atomic ratios based on the Van Krevelen diagram (see Fig. 1).

Moreover, all samples were rich in oxygen functional groups, such as hydroxyl, esters, and carboxyl groups. The presence of oxygen groups is suggested by the bands at 1,710 cm^{-1} (C=O vibrations corresponding to carbonyl, quinone, ester, or carboxyl) [64] and 1,000–1,460 cm^{-1} (C–O stretching vibrations in hydroxyl, ester, or ether and O–H bending vibrations). The increase of the band with the increase of the hydrothermal treatment time resulted in the increase of the intensity of FTIR bands belonging to 1,720 cm^{-1} due to C=O groups. The increase of the oxygen functional groups as were indicated by the increase in the intensity of the bands in the FTIR spectra was also supported by potentiometric titration results, presented in Fig. 5. A difference in the surface charge is observed. The hydrochars present less acidic surface charge with the increase of the hydrothermal treatment time.

3.1.2. Activated carbons

It is noteworthy to mention that after an approximate calculation, the overall yield from waste to activated carbons is nearly 34.5%. The PPH24 hydrochar was further activated with H_3PO_4 at different activation temperatures (400°C, 600°C, and 800°C), and the activated carbons prepared were assigned HP400, HP600, and HP800, respectively. The activated carbons were characterized for their structural and surface properties in order the most efficient to be tested for cobalt ions adsorption from aqueous solutions. The texture of the activated carbons obtained from potato peels hydrochars and chemically activated with H_3PO_4 at three different temperatures (400°C for HP400, 600°C for HP600, and 800°C for HP800) was analyzed by means of nitrogen adsorption–desorption isotherms and is presented in Fig. 6(a); their structural parameters and their specific surface areas are presented in Table 2.

Table 2 shows that these carbons presented a poor porosity. Besides, with the increase of the carbonization temperature a decrease of the BET surface area and microporous volume was noticed, while the carbonization temperature to 800°C resulted in a collapse of structure.

N_2 adsorption–desorption isotherm of the HP400 carbon exhibited an isotherm typical of micromaterials which can be classified as a type I shape (IUPAC classification) [65]. The increase in N_2 adsorption at relative pressure above 0.95 can be attributed to external area. The HP600 carbon exhibited an isotherm typical of microporous materials which can be classified as a type I shape (IUPAC classification). The hysteresis loop presented in the adsorption isotherms of HP600 activated carbon is characteristic of

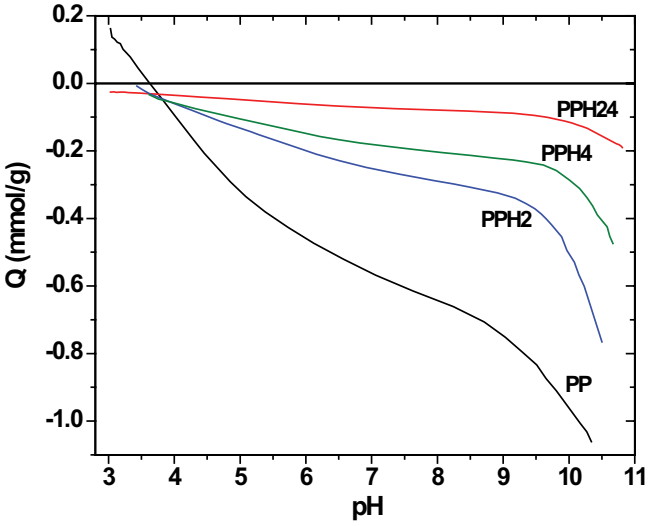

Fig. 5. Potentiometric titration curves of the raw biomass (potato peels) and the hydrochars prepared from potato peels after different time of hydrothermal treatment.

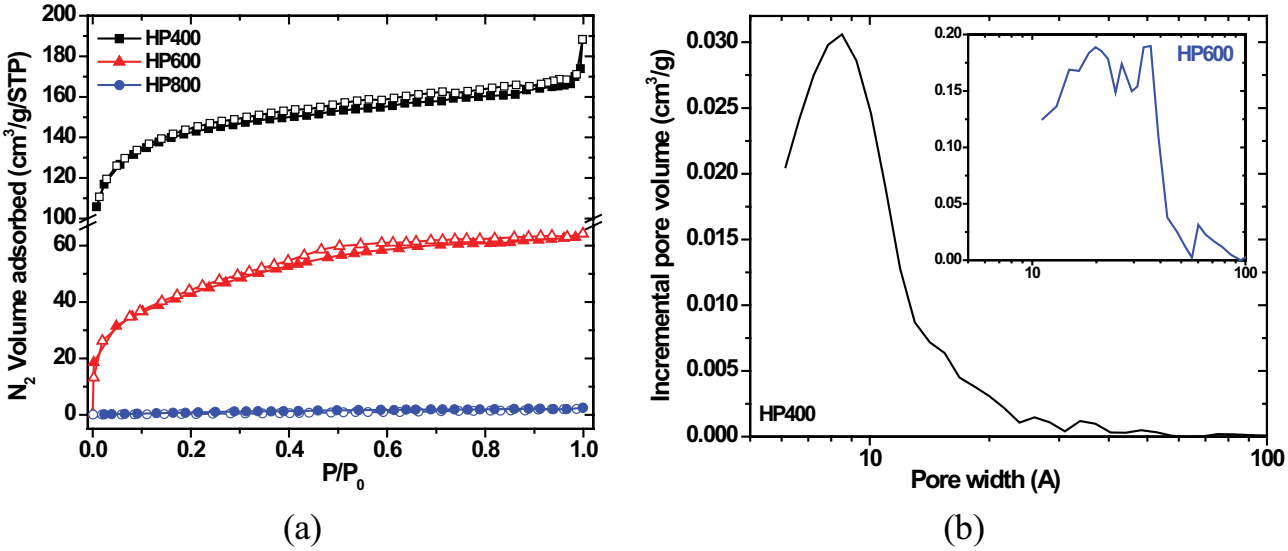

Fig. 6. (a) Nitrogen adsorption–desorption isotherms for activated carbons prepared from hydrochar activated with H_3PO_4 at different activation temperatures (the compact signs are for the adsorption branch and the hollow signs are for the desorption branch); (b) Pore size distribution (DFT) curves for the HP400 and HP600 activated carbons.

Table 2
Structural parameters calculated from nitrogen adsorption isotherms for HP400, HP600, and HP800

Sample	S_{BET} (m^2/g)	V_{MIC} (cm^3/g)	V_{TOT} (cm^3/g)
HP400	465.8	0.142	0.291
HP600	157.3	0.011	0.099
HP800	nd	nd	nd

the coexistence of a small amount of mesopores that are not well defined and ordered [66,67]. The adsorption and desorption branch of the isotherm for the HP800 carbon is presented in the inset of Fig. 6(a)); this type of isotherm is characteristic for nonporous materials [65]. The decrease of microporosity with the increase of the activation temperature could be attributed to violent gasification reactions that take place at activation temperature higher than 500°C that cause the microporous structure to be destroyed by collapsing or combining together [68,69]. For this reason, the activated carbon sample of HP800 was not further examined. The contraction can be due to the catalytic activity of phosphoric acid, causing the growth of polyaromatic clusters. As a result, a densely packed structure is formed and causes loss of porosity. Additionally, by increasing activation temperature up to 800°C, polyphosphates can be progressively formed that can block the pore space decreasing this way the porosity [70]. The pore size distribution for the HP400 and HP600 activated carbons was calculated by applying the DFT method and the results are presented in Fig. 6(b). The results confirmed the microporous structure of the activated carbon HP400 with a maximum at 0.85 nm confirming the narrow pore size distribution for this carbon. HP600 presented micro, mesopores, and macropores, as well (inset of Fig. 6(b)); the distribution reveals the low order of pore formation for this carbon.

SEM images of HP400 and HP600 activated carbons presented in Fig. 7 exhibit a different morphology. HP400 carbon consists of nearly spherical particles of an average size of 0.5 μm as well as adhesions between carbon microspheres. Similar morphology was presented for hydrothermally prepared glycose-based activated carbon [71] and walnut shell derived hydrothermally prepared activated carbons, as well [72]. By increasing the activation temperature the texture of the HP600 carbon becomes compact having this way a smaller surface Area as was estimated by nitrogen adsorption measurements. This morphology was similar with the H_3PO_4 activated carbon prepared after pyrolysis at 600°C [15].

The FTIR spectra of HP400 and HP600 carbons are shown in Fig. 8. The spectra are characteristic of carbonized materials [72] and they differ from that of the hydrochars (Fig. 2). Thus, the carbonized samples exhibit a broad band at around 1,620 cm^{-1} (*G*-mode), which reveal the presence of sp^2 atoms of carbon in benzene or condensed benzene rings of amorphous (partially hydrogenated) carbon [15,72]. Moreover, bands from 900 to 1,300 cm^{-1} are due to C–O bonds (ethers) and to C–OH groups [15,72], while at about 1,400 cm^{-1} are due to lactone groups and at 1,750 cm^{-1} are due to carbonyl groups. From Fig. 8, it is shown that activation temperature increases the amount of oxygen groups as seen by the increased intensity of the bands at ~1,000 and ~1,400 cm^{-1}. The results are consistent with previous findings [15,72]. The HP400 and HP600 carbons were activated with phosphoric acid and additionally present characteristic bands due to phosphorus and phosphor-carbonaceous compounds, that is, at about 1,060 and 990 cm^{-1} [15]. The peak at 990 cm^{-1} more intense for the HP400 carbon can be attributed to P–O–C aromatic or aliphatic stretching, P–O stretching in >P=OOH, P–OH bending, or P–O–P asymmetric stretching in polyphosphates. The peak at 1,060 cm^{-1} more intense for HP600 carbon may be due to the symmetrical vibration in the polyphosphate chain P–O–P or to the P^+–O^- bond in acid phosphate esters [15].

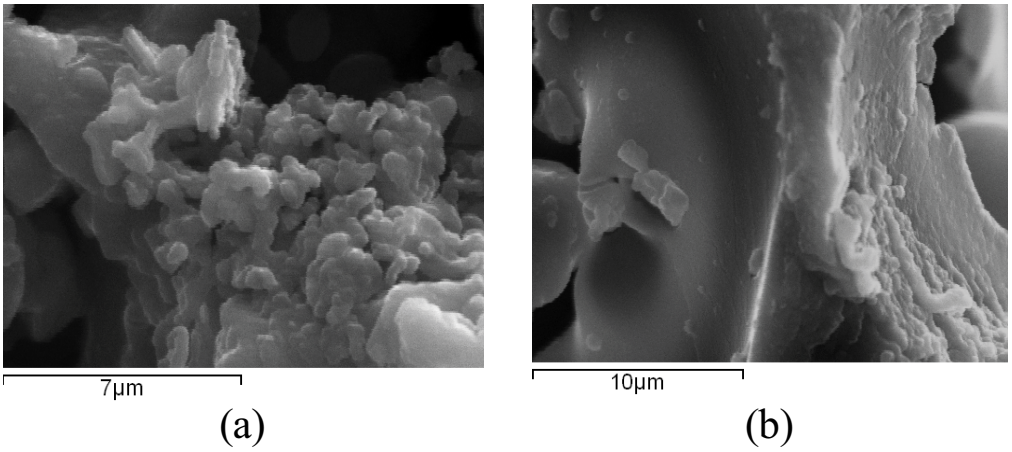

Fig. 7. SEM images of the (a) HP400 and (b) HP600 prepared from potato peels hydrochars.

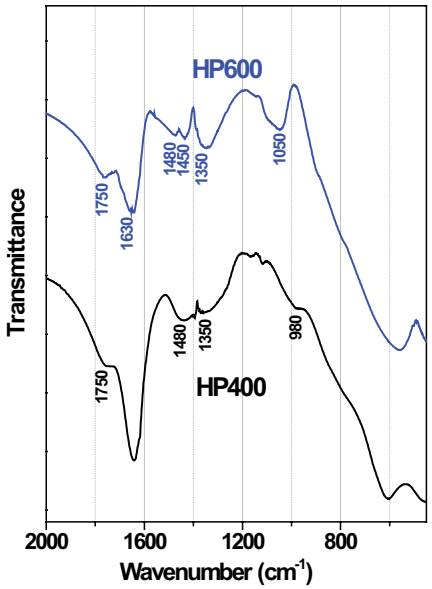

Fig. 8. FTIR spectra of HP400 and HP600 activated carbon samples.

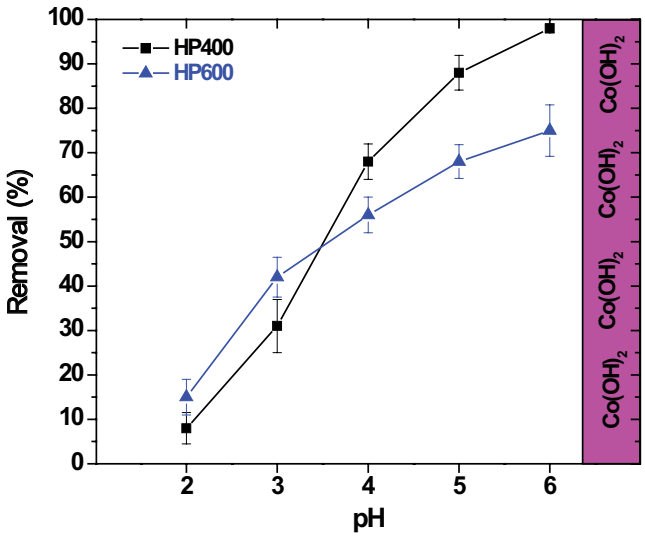

Fig. 9. Effect of pH on Co(II) adsorption onto HP400 and HP600.

3.2. Adsorption evaluation

3.2.1. Effect of pH

One of the most crucial factors, which affect the adsorptive behavior of materials, is the pH of the solution (adsorbate). Therefore, the first parameter investigated is the effect of pH on Co(II) removal. Fig. 9 presents the adsorption behavior of the material in five experimental pH values (2–6).

At strong acidic conditions the removal of Co(II) was very small (8% and 15% for HP400 and HP600, respectively). Then increasing the pH, the removal of ions was suddenly improved for HP400 (31%, 68%, and 88% at pH = 3, 4, and 5, respectively) and also for HP600 (42%, 56%, and 68% at pH = 3, 4, and 5, respectively). But, as it can be seen, the trend of the increase was reversed for the two materials; HP400 more sharply increased its removal now compared with HP600. The higher ion removals were found at pH = 6 (HP400, 98% and HP600, 75%). Some possible explanations about the pH-behavior of the system can be taking into the mind the pH at pH_{zpc} in line with the speciation of Co(II) in solution. It is known that at 2 < pH < 6 pH the cobalt is present as Co^{2+}. The pH at which the charge of the solid surface is zero is referred to as the pH_{zpc}. At pH > pH_{zpc}, the surface of carbon is charged negatively and at pH < pH_{zpc} probably is charged positively. The amount of adsorption at pH > pH_{zpc} was maximum because many interactions of Co^{2+} with the negatively charged adsorbent. At acidic/low pH values, especially at pH < pH_{zpc}, the Co^{2+} species which are positively charged may repel with the carbon surface carrying equal charge and thereby decreases the Co(II) adsorption [15]. Another explanation may be the suppression of the complexation. In some acidic solutions (low pH), some groups can be protonated (or difficult to dissociate); so the complexation/combination among ions and the surficial groups of the carbon are suppressed. Other researchers published similar explanations regarding the effect of pH on the adsorption of ions (heavy metals) on activated carbons [37].

3.2.2. Kinetics

The next factor studied was the effect of contact time on Co(II) adsorption and the different kinetics of the adsorption process for the two materials. It is very important to limit the duration of agitation (meaning energy, cost, money, etc.) and reach the end of adsorption process. The experimental kinetic data/points were fitted to the most widely two kinetic equations; pseudo-first-order and pseudo-second-order equation. It was found that pseudo-second-order model better fitted to the experimental data for both carbons (R^2 = 0.985–0.994). Additionally, it was found that the adsorption process was nearly two times faster for HP400 (k_2 = 0.086 min^{-1}) than HP600 (k_2 = 0.040 min^{-1}) if we compare the kinetic constants. The trend of both kinetic curves was similar; sharp ions removal in the first phase of adsorption (0–60 min), milder/gradual removal in the second phase (60–360), and then a kinetic plateau (equilibrium) was observed, suggesting the end of the process. All above must be carefully taken into consideration since the removal is close to 100% and it is recommended that for an accurate analysis of kinetic data removals should be lower than 95%–90%. As it can be also seen from Figs. 10(b) and (c) Weber–Morris and Elovich did not present good fitting.

3.2.3. Isotherms and adsorption mechanism

The effect of initial ion concentration was studied using fitting isotherm models. Fig. 11 clearly shows that the adsorption capacity is improved with increase of the initial Co(II) concentration from 10 to 1,000 mg/L.

Table 3 presents the equilibrium fitting results after running Langmuir, D–R, and Freundlich models. The best fitting was achieved using Langmuir equation (R^2 = 0.982–0.994), while it is clear that the difference of maximum adsorption capacity (Q_m) is impressively large. In particular, HP400 has approximately two times higher adsorption capacity (479 mg/g) than HP600 (217 mg/g).

To explain this difference, it is mandatory to check the surface area found in characterization (Table 2). As it is widely known, the adsorption mechanism in the case of activated carbons is due to the huge porous network and surface area. Then diffusion phenomena governed the adsorption of ions into the network. The surface area of HP400 was 466 m^2/g,

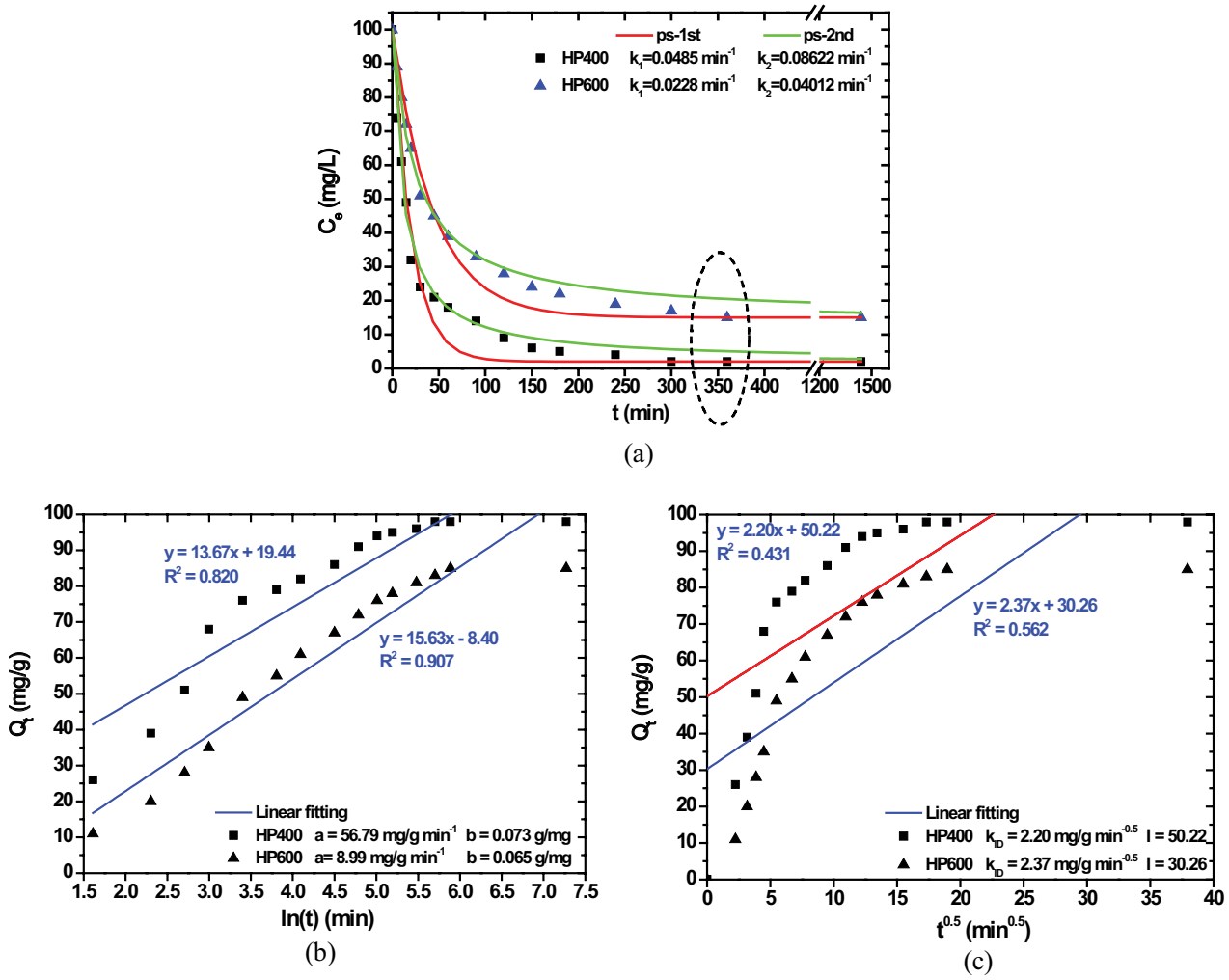

Fig. 10. (a) Effect of contact time on Co(II) adsorption onto HP400 and HP600 (pseudo-first- and pseudo-second-order kinetic equations); (b) Elovich equation; and (c) Weber–Morris equation.

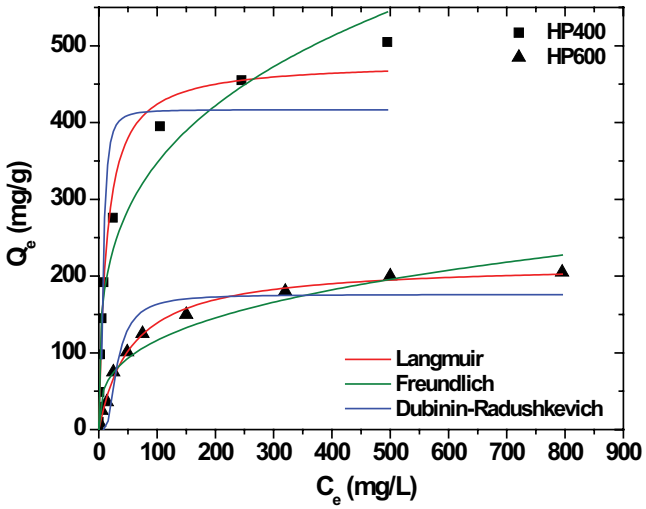

Fig. 11. Effect of initial Co(II) concentration for HP400 and HP600.

while the respective of HP600 was 167 m^2/g. This means that HP400 has approximately three times higher surface area and total pore volume. However, this difference cannot cover the difference of Q_m shown ($Q_{m,HP400} > 2\ Q_{m,HP600}$). The latter implies that many adsorption mechanisms are happened simultaneously and not only diffusion. This can be also confirmed observing the FTIR spectra after Co(II) adsorption (Fig. 12). Considering also the results confirmed by pore size distribution (Fig. 6(b)), it is clear that HP400 with a narrow pore size distribution of a maximum of 0.85 nm is a better adsorbent for the cobalt ion of the similar size.

After Co(II) adsorption (Fig. 12), the band at 1,645 cm^{-1} for HP400 and HP600 carbons shifted to 1,664 cm^{-1}, and 1,673 cm^{-1} for HP400 and HP600 carbons, respectively, mainly due to the dispersive interactions between the pi-electrons of the aromatic ring of HP400 and Co(II) leading to an increased adsorption attributed to ion-exchange reactions between the metal ion and the delocalized protonated π-electrons of the graphene layer (−Cp−H_3O^+) [4] as was also reported for the adsorption of Cr(III), Cd(II) and Hg(II) on activated carbons [70]. FTIR results for spent HP400 and HP600 carbons presented eliminated vibration bands representing O–H and C–O groups due to the dissociation of H^+ leading to the conclusion that during the adsorption Co(II) interacted with the C–O moieties in phenolic and carboxylic groups.

As reported in literature, the reactions that take place during the adsorption of Co(II) on activated carbon are [37]:

$$2(COH) + Co^{2+} \rightleftarrows (CO^-)_2\, Co^{2+} + 2H^+ \quad (11)$$

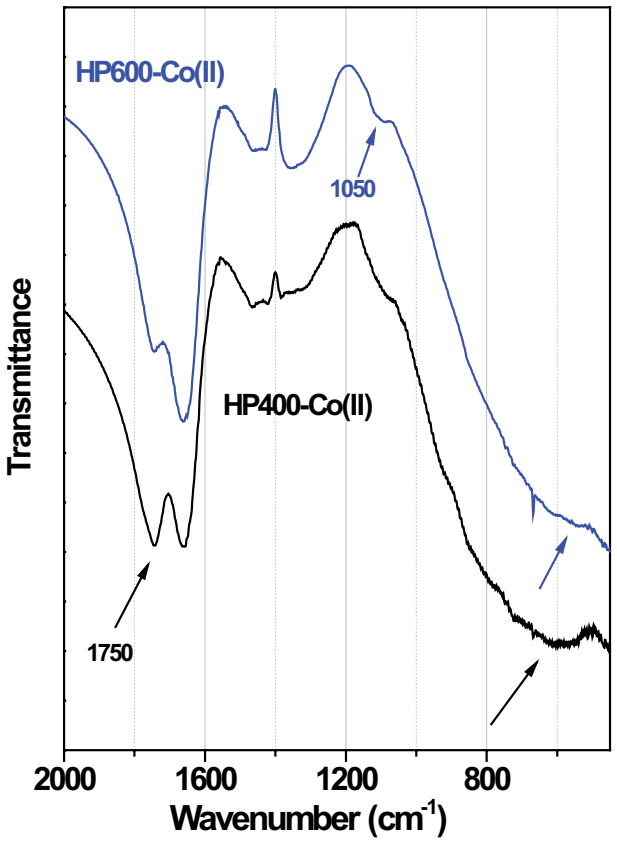

Fig. 12. FTIR spectra of HP400 and HP600 activated carbon samples after Co(II) adsorption.

$$2CO^- + Co^{2+} \rightleftarrows (CO^-)_2\, Co^{2+} \quad (12)$$

where C is for solid surface.

These interactions may happen through noncovalent bonding or just nonchemically covalent bonding. Co^{2+} cations probably replaced the H^+ of the phenol and carboxyl groups, and attached on the C–O groups with electrovalent bond. Based on the above results, it is concluded that H_3PO_4 activation introduced oxygen functional groups, which provided active binding sites for cobalt that was adsorbed on these carbon surface by electrostatic interaction cation exchange, and surface complexation mechanisms. The above-presented results suggest that activated carbon from potato peels, activated with phosphoric acid have a considerable promise for heavy metal ion removal, and as a consequence the water purification.

Table 3
Equilibrium parameters for the adsorption of Co(II) onto HP400 and HP600

Sample	Langmuir equation			Freundlich equation			Dubinin–Radushkevich		
	Q_m (mg/g)	K_L (L/g)	R^2 (–)	K_F ($mg^{1-1/n}\,L^{1/n}\,g^{-1}$)	n (–)	R^2 (–)	Q_m (mg/g)	B_D (mg)	R^2 (–)
HP400	479	0.07641	0.982	95.65	3.57	0.866	417	7.38×10^{-6}	0.875
HP600	217	0.01782	0.994	26.27	3.09	0.851	176	1.21×10^{-4}	0.894

4. Conclusions

This paper investigates the synthesis of activated carbons with hydrothermal treatment (at three different time intervals 2, 4, and 24 h) from zero-cost sources (potato peels), and activation with H_3PO_4 (at three different temperatures 400°C, 600°C, and 800°C). According to characterizations, HP800 presented negligible surface area and for this reason was not further examined from adsorption process. Equilibrium and kinetic experiments were carried out at the optimum found pH (6). HP400 had approximately two times higher adsorption capacity (479 mg/g) than HP600 (217 mg/g), while the surface area of the former (466 m^2/g) three times higher than that of 600°C (167 m^2/g). The possible adsorption mechanism was proposed based on FTIR spectra taken after the adsorption of Co(II). Based on the above results, H_3PO_4 activation introduced oxygen functional groups, which provided active binding sites for cobalt that was adsorbed on these carbon surfaces by electrostatic interaction cation exchange, and surface complexation mechanisms.

Conflicts of interest

The authors declare no conflict of interest.

References

[1] G.Z. Kyzas, Green Adsorbents. Bentham Science Publishers, United Arab Emirates, 2015.
[2] G.Z. Kyzas, Coffee Wastes as Adsorbents, C.N. Foster, Ed., Agricultural Wastes: Characteristics, Types and Management, Noc, New York, USA, 2015, pp. 215–229.
[3] J.R. Perrich, Activated Carbon Adsorption for Wastewater Treatment, CRC Press, Boca Raton, FL, 1981.
[4] J.S. Mattson, H.B. Mark, Activated Carbon: Surface Chemistry and Adsorption from Solution, Marcel Dekker, New York, 1971.
[5] R.C. Bansal, M. Goyal, Activated Carbon Adsorption. CRC Press, Taylor & Francis, Boca Raton, FL, USA, 2005.
[6] R. Mailler, J. Gasperi, Y. Coquet, S. Deshayes, S. Zedek, C. Cren-Olivé, N. Cartiser, V. Eudes, A. Bressy, E. Caupos, R. Moilleron, G. Chebbo, V. Rocher, Study of a large scale powdered activated carbon pilot: removals of a wide range of emerging and priority micropollutants from wastewater treatment plant effluents, Water Res., 72 (2015) 315–330.
[7] I. Anastopoulos, G.Z. Kyzas, Agricultural peels for dye adsorption: a review of recent literature, J. Mol. Liq., 200 (2014) 381–389.
[8] I. Anastopoulos, G.Z. Kyzas, Progress in batch biosorption of heavy metals onto algae, J. Mol. Liq., 209 (2015) 77–86.
[9] I. Anastopoulos, G.Z. Kyzas, Composts as biosorbents for decontamination of various pollutants: a review, Water Air Soil Pollut., 226 (2015) 61.
[10] E.A. Deliyanni, G.Z. Kyzas, K.S. Triantafyllidis, K.A. Matis, Activated carbons for the removal of heavy metal ions: a systematic review of recent literature focused on lead and arsenic ions, Open Chem., 13 (2015) 699–708.
[11] G.Z. Kyzas, A decolorization technique with spent "greek coffee" grounds as zero-cost adsorbents for industrial textile wastewaters, Materials, 5 (2012) 2069–2087.
[12] G.Z. Kyzas, Commercial coffee wastes as materials for adsorption of heavy metals from aqueous solutions, Materials, 5 (2012) 1826–1840.
[13] G.Z. Kyzas, E.A. Deliyanni, Modified activated carbons from potato peels as green environmental-friendly adsorbents for the treatment of pharmaceutical effluents, Chem. Eng. Res. Des., 97 (2015) 135–144.
[14] G.Z. Kyzas, E.A. Deliyanni, N.K. Lazaridis, Magnetic modification of microporous carbon for dye adsorption, J. Colloid Interface Sci., 430 (2014) 166–173.
[15] G.Z. Kyzas, E.A. Deliyanni, K.A. Matis, Activated carbons produced by pyrolysis of waste potato peels: cobalt ions removal by adsorption, Colloid Surf. A., 490 (2016) 74–83.
[16] I. Anastopoulos, M. Karamesouti, A.C. Mitropoulos, G.Z. Kyzas, A review for coffee adsorbents, J. Mol. Liq., 229 (2017) 555–565.
[17] M.M. Koutlemani, P.Mavros, A.I. Zouboulis, K.A. Matis, Recovery of co^{2+} ions from aqueous solutions by froth flotation, Sep. Sci. Technol., 29 (1994) 867–886.
[18] N. Barrak, R. Mannai, M. Zaidi, S. Achour, M. Kechida, A.N. Helal, Optimization of novacron blue 4r (nb4r) removal by adsorption process on activated carbon using response surface methodology, Desal. Wat. Treat., 104 (2018) 346–353.
[19] L. Daddi Oubekka, N.E. Djelali, V. Chaleix, V. Gloaguen, Removal of lead (ii) and cadmium (ii) from aqueous solutions by adsorption on date pits modified by DTPAD, Desal. Wat. Treat., 98 (2017) 233–243.
[20] W. Liu, J. Zhang, N. Li, Q. Ping, Adsorption of heavy metal ions with modified diatomite from effluent, Desal. Wat. Treat., 103 (2018) 216–220.
[21] F. Medjdoub, K. Louhab, A. Hamouche, Comparative study of the adsorption of paracetamol from aqueous solution on olive stones and date pits, Desal. Wat. Treat., 104 (2018) 225–233.
[22] A.A. Peláez Cid, A.M.H. González, M.S. Villanueva, Adsorption of heavy metals on activated carbons and their respective lignocellulosic precursors: experimental and theoretical approach, Desal. Wat. Treat., 104 (2018) 169–174.
[23] Y. Rong, H. Li, L. Xiao, Q. Wang, Y. Hu, S. Zhang, R. Han, Adsorption of malachite green dye from solution by magnetic activated carbon in batch mode, Desal. Wat. Treat., 106 (2018) 273–284.
[24] Z. Roostan, A. Rashidi, S.M. Borghei, Nickel ion removal from aqueous solution using recyclable zeolitic imidazolate framework-8 (zif-8) nano adsorbent: a kinetic and equilibrium study, Desal. Wat. Treat., 103 (2018) 141–151.
[25] T. Satapanajaru, C. Chokejaroenrat, P. Pengthamkeerati, Removal of reactive black 5 and its degradation using combined treatment of nano-zerovalent iron activated persulfate and adsorption processes, Desal. Wat. Treat., 102 (2018) 300–311.
[26] F. Xiao, J. Cheng, X. Fan, C. Yang, Y. Hu, Adsorptive removal of the hazardous anionic dye congo red and mechanistic study of zif-8, Desal. Wat. Treat., 101 (2018) 291–300.
[27] X. Zhang, M. Qiao, Z. Zhang, R. Song, Z. Li, H. Li, Removal of zn(ii) from aqueous solutions by adsorption using different types of waste bricks, Desal. Wat. Treat., 106 (2018) 177–190.
[28] M.A. Zulfikar, Mustapa, M.B. Amran, A. Alni, D. Wahyuningrum, Adsorption of cationic dye from aqueous solution using molecularly imprinted polymers (MIPs). Desal. Wat. Treat., 103 (2018) 102–112.
[29] R. Ahmad, I. Hasan, A. Mittal, Adsorption of cr (vi) and cd (ii) on chitosan grafted polyaniline-ommt nanocomposite: isotherms, kinetics and thermodynamics studies, Desal. Wat. Treat., 58 (2017) 144–153.
[30] A.H. Jawad, N.F.H. Mamat, M.F. Abdullah, K. Ismail, Adsorption of methylene blue onto acid-treated mango peels: kinetic, equilibrium and thermodynamic study, Desal. Wat. Treat., 59 (2017) 210–219.
[31] P. Vairavel, V. Ramachandra Murty, S. Nethaji, Removal of congo red dye from aqueous solutions by adsorption onto a dual adsorbent (neurospora crassa dead biomass and wheat bran): optimization, isotherm, and kinetics studies, Desal. Wat. Treat., 68 (2017) 274–292.
[32] L. Wu, Z. Qin, F. Yu, J. Ma, Graphene oxide cross-linked chitosan nanocomposite adsorbents for the removal of cr (vi) from aqueous environments, Desal. Wat. Treat., 72 (2017) 300–307.
[33] M.J. Angove, B.B. Johnson, J.D. Wells, The influence of temperature on the adsorption of cadmium(ii) and cobalt(ii) on kaolinite, J. Colloid Interface Sci., 204 (1998) 93–103.
[34] E.H. Borai, M.M.E. Breky, M.S. Sayed, M.M. Abo-Aly, Synthesis, characterization and application of titanium oxide nanocomposites for removal of radioactive cesium, cobalt and europium ions, J. Colloid Interface Sci., 450 (2015) 17–25.

[35] J.D. Wells, B.B. Johnson, The influence of temperature on the adsorption of cadmium(ii) and cobalt(ii) on goethite. J. Colloid Interface Sci., 211 (1999) 281–290.
[36] A.H. Sulaymon, B.A. Abid, J.A. Al-Najar, Removal of lead copper chromium and cobalt ions onto granular activated carbon in batch and fixed-bed adsorbers, Chem. Eng. J., 155 (2009) 647–653.
[37] K.A. Krishnan, T.S. Anirudhan, Kinetic and equilibrium modelling of cobalt(ii) adsorption onto bagasse pith based sulphurised activated carbon, Chem. Eng. J., 137 (2008) 257–264.
[38] M. Abbas, S. Kaddour, M. Trari, Kinetic and equilibrium studies of cobalt adsorption on apricot stone activated carbon, J. Ind. Eng. Chem., 20 (2014) 745–751.
[39] B. Boulinguiez, P. Le Cloirec, Adsorption/desorption of tetrahydrothiophene from natural gas onto granular and fiber-cloth activated carbon for fuel cell applications, Energy Fuels, 23 (2009) 912–919.
[40] C. Lastoskie, K.E. Gubbins, N. Quirke, Pore size distribution analysis of microporous carbons: a density functional theory approach, J. Phys. Chem., 97 (1993) 4786–4796.
[41] P.I. Ravikovitch, S.C.O. Domhnaill, A.V. Neimark, F. Schueth, K.K. Unger, Capillary hysteresis in nanopores: theoretical and experimental studies of nitrogen adsorption on mcm-41, Langmuir, 11 (1995) 4765–4772.
[42] L.H. Cohan, Sorption hysteresis and the vapor pressure of concave surfaces, J. Am. Chem. Soc., 60 (1938) 433–435.
[43] S. Brunauer, P.H. Emmett, E. Teller, Adsorption of gases in multi-molecular layers, J. Am. Chem. Soc., 60 (1938) 309–319.
[44] E.P. Barrett, L.G. Joyner, P.P. Halenda, The determination of pore volume and area distributions in porous substances. I. Computations from nitrogen isotherms, J. Am. Chem. Soc., 73 (1951) 373–380.
[45] M. Sevilla, A.B. Fuertes, The production of carbon materials by hydrothermal carbonization of cellulose, Carbon, 47 (2009) 2281–2289.
[46] A.M. Donia, A.A. Atia, K.Z. Elwakeel, Selective separation of mercury(ii) using magnetic chitosan resin modified with schiff's base derived from thiourea and glutaraldehyde, J. Hazard. Mater., 151 (2008) 372–379.
[47] I. Langmuir, The adsorption of gases on plane surfaces of glass, mica and platinum, J. Am. Chem. Soc., 40 (1918) 1361–1403.
[48] H. Freundlich, Over the adsorption in solution. Z. Phys. Chem., 57 (1906) 385–470.
[49] M.M. Dubinin, L.V. Radushkevich, Equation of the characteristic curve of activated charcoal, Proc. Acad. Sci. USSR, 55 (1947) 331–333.
[50] S. Lagergren, About the theory of so-called adsorption of soluble substances, Handlingar, 24 (1898) 1–39.
[51] Y.S. Ho, J.C.Y. Ng, G. McKay, Kinetics of pollutant sorption by biosorbents: review, Sep. Purif. Methods, 29 (2000) 189–232.
[52] S. Azizian, Kinetic models of sorption: a theoretical analysis, J. Colloid Interface Sci., 276 (2004) 47–52.
[53] M. Sevilla, A.B. Fuertes, Chemical and structural properties of carbonaceous products obtained by hydrothermal carbonization of saccharides, Chem. Eur. J., 15 (2009) 4195–4203.
[54] X. Liang, M. Zeng, C. Qi, One-step synthesis of carbon functionalized with sulfonic acid groups using hydrothermal carbonization, Carbon, 48 (2010) 1844–1848.
[55] S. Zhao, X.-Y. Li, C.-Y. Wang, M.-M. Chen, Preparation of bowl-like and eggshell-like hollow carbon microspheres from potato starch, Mater. Lett., 70 (2012) 54–56.
[56] G.K. Parshetti, S. Kent Hoekman, R. Balasubramanian, Chemical, structural and combustion characteristics of carbonaceous products obtained by hydrothermal carbonization of palm empty fruit bunches, Bioresour. Technol., 135 (2013) 683–689.
[57] L. Yu, C. Falco, J. Weber, R.J. White, J.Y. Howe, M.-M. Titirici, Carbohydrate-derived hydrothermal carbons: a thorough characterization study, Langmuir, 28 (2012) 12373–12383.
[58] M.-M. Titirici, M. Antonietti, Chemistry and materials options of sustainable carbon materials made by hydrothermal carbonization, Chem. Soc. Rev., 39 (2010) 103–116.
[59] L. Zhang, W. Xie, X. Zhao, Y. Liu, W. Gao, Study on the morphology, crystalline structure and thermal properties of yellow ginger starch acetates with different degrees of substitution, Thermochim. Acta, 495 (2009) 57–62.
[60] M. Sevilla, J.A. Maciá-Agulló, A.B. Fuertes, Hydrothermal carbonization of biomass as a route for the sequestration of CO_2: chemical and structural properties of the carbonized products, Biomass Bioenergy, 35 (2011) 3152–3159.
[61] X. Sun, Y. Li, Colloidal carbon spheres and their core/shell structures with noble-metal nanoparticles, Angew. Chem. Int. Ed., 43 (2004) 597–601.
[62] H.R. Holgate, J.C. Meyer, J.W. Tester, Glucose hydrolysis and oxidation in supercritical water. AIChE J., 41 (1995) 637–648.
[63] A.C. Lua, T. Yang, Effect of activation temperature on the textural and chemical properties of potassium hydroxide activated carbon prepared from pistachio-nut shell, J. Colloid Interface Sci., 274 (2004) 594–601.
[64] B.M. Kabyemela, T. Adschiri, R.M. Malaluan, K. Arai, Glucose and fructose decomposition in subcritical and supercritical water: detailed reaction pathway, mechanisms, and kinetics, Ind. Eng. Chem. Res., 38 (1999) 2888–2895.
[65] J. Rouquerol, D. Avnir, C.W. Fairbridge, D.H. Everett, J.M. Haynes, N. Pernicone, J.D.F. Ramsay, K.S.W. Sing, K.K. Unger, Recommendations for the characterization of porous solids (technical report), Pure Appl. Chem., 66 (1994) 1739–1758.
[66] M. Chen, D. Yan, X. Zhang, Z. Yu, G. Zhu, Y. Zhao, S. Lu, G. Chen, H. Xu, A. Yu, Activated carbons by a hydrothermal-assisted activated method for li-ion batteries, Mater. Lett., 196 (2017) 276–279.
[67] W. Yuan, A. Xie, S. Li, F. Huang, P. Zhang, Y. Shen, High-activity oxygen reduction catalyst based on low-cost bagasse, nitrogen and large specific surface area, Energy, 115 (2016) 397–403.
[68] F. Suárez-García, A. Martínez-Alonso, J.M.D. Tascón, Pyrolysis of apple pulp: chemical activation with phosphoric acid, J. Anal. Appl. Pyrolysis, 63 (2002) 283–301.
[69] F. Suárez-García, S. Villar-Rodil, C.G. Blanco, A. Martínez-Alonso, J.M.D. Tascón, Effect of phosphoric acid on chemical transformations during nomex pyrolysis, Chem. Mater., 16 (2004) 2639–2647.
[70] M. Myglovets, O.I. Poddubnaya, O. Sevastyanova, M.E. Lindström, B. Gawdzik, M. Sobiesiak, M.M. Tsyba, V.I. Sapsay, D.O. Klymchuk, A.M. Puziy, Preparation of carbon adsorbents from lignosulfonate by phosphoric acid activation for the adsorption of metal ions, Carbon, 80 (2014) 771–783.
[71] Z. Chen, L. Ma, S. Li, J. Geng, Q. Song, J. Liu, C. Wang, H. Wang, J. Li, Z. Qin, S. Li, Simple approach to carboxyl-rich materials through low-temperature heat treatment of hydrothermal carbon in air, Appl. Surf. Sci., 257 (2011) 8686–8691.
[72] S. Román, J.M. Valente Nabais, B. Ledesma, J.F. González, C. Laginhas, M.M. Titirici, Production of low-cost adsorbents with tunable surface chemistry by conjunction of hydrothermal carbonization and activation processes, Micropor. Mesopor. Mater., 165 (2013) 127–133.
[73] M. Sánchez-Polo, J. Rivera-Utrilla, Adsorbent-adsorbate interactions in the adsorption of cd(ii) and hg(ii) on ozonized activated carbons, Environ. Sci. Technol., 36 (2002) 3850–3854.